King's College London

Department of Mathematics

Plagiarism Statement for Coursework

The following statement must be signed by all students submitting dissertations, projects or essays as a part of their formal assessments for any degree.

Student Name: Robert Michael Jones

Module Code: 7CCMNE07

Title of Project/Dissertation: Research Methods for Theoretical Modelling of Non-Equilibrium Systems Ergodicity breaking in many body localised systems and violations of the Eigenstate Thermalisation Hypothesis

DECLARATION:

I have read and understood the above statement and the College's statement on Academic Honesty and Integrity. I declare that the content of this submission is my own work.

I understand that plagiarism is a serious examination offence, an allegation of which can result in action being taken under the College's Misconduct regulations.

Signature: Date: 13/04/2019

Please submit <u>one</u> copy of the plagiarism declaration with your project/essay

Research Methods for Theoretical Modelling of Non-Equilibrium Systems
Ergodicity breaking in many body localised systems

Robert Jones - 1869143 -

Abstract

We are studying closed quantum systems which are able to evade thermalisation by becoming localised due to the presence of random, quenched disorder. We consider such systems via methods of basis transformations to demonstrate agreement with the Anderson insulator and numerical simulations of time dependent observables. Principally, we are interested in: the propagation and saturation of entanglement entropy; and the level spacing distribution of the many-body Hamiltonian's energy eigenvalues.

1 Introduction

In a sufficiently long stretch of time, one expects a physical system to reach a state of equilibrium. In statistical physics, we call such systems ergodic - they are able to explore all phase space configurations as permitted by globally conserved quantities with the only measurable quantities being governed by a small number of extensive parameters of the system. E.g., temperature and chemical potential.

It is currently believed that the mechanism by which a closed quantum system may thermally equilibrate is for each subsystem of the whole to thermalise with respect to the rest of the system by a process known as the eigenstate thermalisation hypothesis (ETH). That is to say, the system may behave as its own heat and particle bath meaning that such systems may be faithfully represented by both the micro-canonical ensemble and the grand canonical ensemble. A consequence of this is that all information regarding the initial state is distributed around the entire system during thermalisation. If one wished to measure a local property of the initial state, e.g., the orientation of an arbitrary spin, then one must measure a non-physical global observable as information regarding that individual spin will have decohered across the whole system. This is the process of quantum decoherence and is a consequence of the ETH.

There has been much interest in the phenomenon of exponentially localised degrees of freedom, initiated by the seminal work of Anderson [1]. From here, the notion of localisation has been developed via a variety of numerical tests; analytic arguments and experimental realisations of systems permitting many-body interactions in the presence of random disorder (i.e., most physical systems).

1.1 Eigenstate thermalisation hypothesis

The ETH is defined in [2] and [3]; "In ergodic systems, the individual excited eigenstates have thermal expectation values of physical observables, which are identical to those obtained using the microcanonical and Gibbs ensembles". That is to say that in the thermal regime, the local measurement of a quantity, such as energy, will correspond to the thermal equilibrium energy at a temperature T. If $H|E_n\rangle = E_n|E_n\rangle$, then $E_n = \langle H \rangle_{T_n}$ for the nth energy eigenvalue of the Hamiltonian H. Furthermore, if the system is instantaneously in this eigenstate, characterised by temperature, T_n, then its density operator will be given by $\rho = |E_n\rangle\langle E_n| = \frac{1}{Z}e^{-\frac{H}{K_B T}}$. The thermal density operator at temperature T. Moreover, energy transport is necessary in thermalising systems so that they may explore all configurations of their phase space permitted by conservation laws, i.e., behave ergodically.

1.2 Phenomenology of localisation

Anderson initially introduced the notion of quantum localisation [1] with a single particle propagating on a disordered lattice in arbitrary spatial dimensions. Such systems can be described by the following tight binding Hamiltonian

$$H = t\sum_{\langle ij \rangle}\left(c_i^\dagger c_j + c_j^\dagger c_i\right) + \sum_i \mu_i c_i^\dagger c_i \qquad (1)$$

where $c_i^\dagger$ and c_i respectively create and destroy spinless fermionic modes and μ_i is a random chemical potential. In the absence of a perturbation, the energy eigenstates of this Hamiltonian are Bloch waves freely propagating. In three dimensions with strong disorder, or in fewer than three dimensions with any disorder; the eigenstates of this Hamiltonian become exponentially localised around some point R_α in the lattice;

$$\{\psi_\alpha\} \propto e^{-\frac{\{r - R_\alpha\}}{\xi_0}} \qquad (2)$$

where ξ_0 is the localisation length. When localised, transport is stunted - currents cannot diffuse across the lattice. Hence the system behaves as an (Anderson) insulator.

Extending this notion to the many body localised (MBL) regime requires the introduction of weak, short-range, two body interactions to the Anderson model above. These interactions must be weak, relative to the perturbation in order for the many-body eigenstates to become localised.

Phenomenologically speaking, we observe the breaking of ergodicity in such models due to a collection of quasi-local integrals of motion (LIOM)[9][22][23][20]. By integral of motion, we mean that there is a quantity which commutes with the Hamiltonian. Integrable systems are defined as those which have an infinite number of conservation laws [12] resulting in an infinite number of constants of motion.

In the context of MBL, our LIOMs arise from quasi-local spin operators defined as

$$\tau_i^z = \mathcal{U}\sigma_i^z\mathcal{U}^\dagger \qquad (3)$$

where $\mathcal{U}$ is the unitary transformation which diagonalises the system's Hamiltonian, $H_{Diag} = \mathcal{U}^\dagger H \mathcal{U}$ in the spin up, down basis. When analytically considering these transformations, one may take the weak-coupling limit and construct the quasi-local unitary transformations perturbatively [16]. These LIOMs are centred on their corresponding physical spin operator and only interact with spins in some finite region of space (support) decaying off exponentially. This exponentially decaying support is due to the quasi-local nature of the unitary transformations, in the presence of sufficient disorder, and explains the exponential suppres-

sion of transport in the MBL phase.

One may demonstrate commutation of these LIOMs with the Hamiltonian in a simple argument;

$$H = \mathcal{U} H_{Diag} \mathcal{U}^\dagger \text{ and } \tau_i^z = \mathcal{U} \sigma_i^z \mathcal{U}^\dagger$$

$$[\tau_i^z, H] = [\mathcal{U} \sigma_i^z \mathcal{U}^\dagger, \mathcal{U} H_{Diag} \mathcal{U}^\dagger] =$$

$$(\mathcal{U} \sigma_i^z \mathcal{U}^\dagger \mathcal{U} H_{Diag} \mathcal{U}^\dagger) - (\mathcal{U} H_{Diag} \mathcal{U}^\dagger \mathcal{U} \sigma_i^z \mathcal{U}^\dagger) = \quad (4)$$

$$= \mathcal{U} \sigma_i^z H_{Diag} \mathcal{U}^\dagger - \mathcal{U} H_{Diag} \sigma_i^z \mathcal{U}^\dagger$$

$$= \mathcal{U} [\sigma_i^z, H_{Diag}] \mathcal{U}^\dagger = 0$$

As H_{Diag} is diagonal in the σ^z basis and by definition of unitary transformation, $\mathcal{U}\mathcal{U}^\dagger = \mathbb{I}$.

$$\tau_i^z = U \sigma_i^z U^\dagger$$

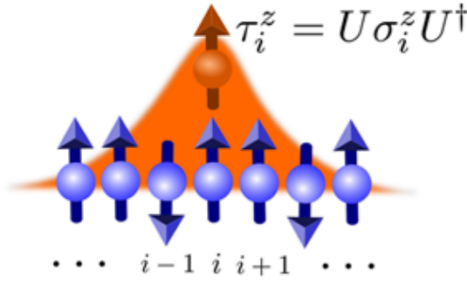$$\cdots \quad i-1 \quad i \quad i+1 \quad \cdots$$

Figure 1: Graphical representation of the quasi-local integral of motion as an effective spin with exponentially decaying support. Image from [2].

2 The model

In the literature, many models have been demonstrated to support MBL behaviour [26][6][5][3]. For the purposes of this research, we shall focus on the spin - $\frac{1}{2}$ XXZ model in the presence of a random longitudinal field. We model the Hamiltonian and many-body eigenstates in the spin $-\frac{1}{2}$ basis orientated in the z direction. $|\uparrow\rangle = (1, 0)$ and $|\downarrow\rangle = (0, 1)$.

$$H_{spin} = J \sum_{i=1}^{N-1} \sigma_i^x \sigma_{i+1}^x + \sigma_i^y \sigma_{i+1}^y + V \sum_{i=1}^{N-1} \sigma_i^z \sigma_{i+1}^z + \sum_{i=1}^{N} h_i \sigma_i^z \quad (5)$$

Where σ_i^α is the αth Pauli matrix acting on a spin at location i, respecting the commutation law, $[\sigma_j^\alpha, \sigma_i^\beta] = \epsilon^{\alpha\beta\gamma}\delta_{ij}\sigma j^\gamma$; δ_{ij} is the Kronecker delta function, and $\epsilon^{\alpha\beta\gamma}$ is the Levi-Cevita operator. All work in this report will use J=2V=1. We interpret h_i as a random magnetic field with site dependent strength, h_i, drawn from a uniform distribution of width $[-h, h]$.

When V = 0, note that (5) will describe a free particle in a random transverse field; the Anderson insulator described in (1). As discussed in section 1.2, the introduction

of a random, longitudinal field coupling to each degree of freedom causes the spins to become exponentially localised about a given lattice point. As we then introduce spin flip interactions by perturbatively turning on V, information regarding the initial state of an arbitrary spin gets transported around the system diffusively in the limit of weak h. This is the mechanism by which the XXZ model thermalises via the ETH.

For sufficient disorder, $h \approx 3.5J$, transport becomes suppressed due to the emergence of LIOMs. In the context of our XXZ model, the explicit form is given by

$$\tau_i^z = \sigma_i^z + \sum_{j,k} \sum_{a,b=x,y,z} f_{i;jk}^{ab} \sigma_j^a \sigma_k^b + \cdots \quad (6)$$

with spin-spin weights decaying exponentially with distance

$$f_{i;jk} \propto e^{-\frac{max|i-j|,|i-k|}{\xi}} \quad (7)$$

Spatial decay of τ_i^z from position i is governed by the many-body localisation length ξ. As is discussed by Abanin and Papic [2], this characteristic length is not the only one to appear in the context of MBL physics and indeed there are others being studied [20] to evaluate behaviour at the point of transition. However; for this work, we shall principally consider systems which are deep in one phase and not at the point of phase transition. The Unitary transformations used in (3) are highly non-local in the thermal regime and so there is no exponential decay of coefficients; hence the LIOMs cease to be quasi-local.

When deep in the localised phase, we note that due to τ_i^z being an integral of motion, its expectation value should remain unchanged during unitary time evolution.

$$\langle \tau_i^z(0) \rangle = \langle \tau_i^z(t) \rangle. \quad (8)$$

Alternatively, $\tau_i^{x,y}$ are not integrals of motion and so it is expected that their amplitudes decay as power law in time [5]. Relating this to the physical spins $\langle \sigma_i^\alpha \rangle$, one may see the coherence of the LIOMs in the coherence of the time dependent signal of the local observable. As we shall explore later in this text, this is a consequence of a non-trivial overlap with the quasi-local LIOMs.

3 Mapping to fermions

As discussed in section 2, it is possible to recast (5) in the form of spinless fermions hopping on a 1D lattice. To do so, we use the Jordan-Wigner transformation defined in [10]:

$$S_j^+ = c_j^\dagger e^{i\pi \sum_i^{i<j} c_i^\dagger c_i}$$

$$S_j^- = e^{-i\pi \sum_i^{i<j} c_i^\dagger c_i} c_j \quad (9)$$

$$S_j^z = c_j^\dagger c_j - \frac{1}{2}$$

Where $S_j^\pm = \frac{1}{2}(\sigma_j^x \pm i\sigma_j^y)$ raises or lowers the spin of a lattice site j by unity; $c_j^\dagger$ and c_j respectively create or destroy a fermion on a lattice site j.

By reversing the definition for $S_j^{\pm}$, we may arrive at the following,

$$\sigma_j^x = (S_j^+ + S_j^-) \ \ i\sigma_j^y = (S_j^+ - S_j^-) \tag{10}$$

These reformulations may then be plugged into (5).

$$\sigma_j^x \sigma_{j+1}^x = (S_j^+ + S_j^-)(S_{j+1}^+ + S_{j+1}^-)$$
$$-\sigma_j^y \sigma_{j+1}^y = (S_{j+1}^+ - S_{j+1}^-) \tag{11}$$
$$\sigma_j^x \sigma_{j+1}^x + \sigma_j^y \sigma_{j+1} = \frac{1}{2}\left(S_j^+ S_{j+1}^- + S_j^- S_{j+1}^+\right)$$

Hence we fully recast (5) in terms of fermionic operators.

$$H = \sum_{j=1}^{N-1} \frac{J}{2}\left(S_j^+ S_{j+1}^- + S_j^- S_{j+1}^+\right) + V\sum_{j=1}^{N-1} Sj^z S_{j+1}^z$$

$$+ \sum_{j=1}^{N} h_j Sj^z =$$

$$= \frac{J}{2}\sum_{j}^{N-1} c_j^\dagger e^{i\pi\sum_i^{i<j} c_i^\dagger c_i} e^{-i\pi\sum_j^{i=j} c_i^\dagger c_i} c_{j+1} \tag{12}$$

$$+ e^{-i\pi\sum_j^{i<j} c_i^\dagger c_i} c_j c_{j+1}^\dagger e^{i\pi\sum_i^{i=j} c_i^\dagger c_i}$$

$$+ V\sum_j^{N-1} \rho_j \rho_{j+1} + \sum_j^{N} \mu_j \rho_j$$

where we are defining $\rho_j = c_j^\dagger c_j - \frac{1}{2}$ as the fermion density operator for a site j. By noting that $S_j^+ S_{j+1}^- = \left(S_j^- S_{j+1}^+\right)^\dagger$, it becomes apparent that we need evaluate only one of these terms and then take the hermitian conjugate of it.

$$S_j^+ S_{j+1}^- = c_j^\dagger e^{i\pi\sum_i^{i<j} c_i^\dagger c_i} e^{-i\pi\sum_j^{i=j} c_i^\dagger c_i} c_{j+1} =$$

$$= c_j^\dagger e^{i\pi c_j^\dagger c_j} c_{j+1} = c_j^\dagger c_{j+1} \tag{13}$$

This is due to the fact that $c_j^\dagger$ is only non-trivial if the jth state is unoccupied, $c_j^\dagger |\ldots n_j \neq 0 \ldots\rangle = 0$. If $n_j = 0$, then the exponent is trivially evaluated to be unity and so we recover the expected result. By then applying our observation of hermiticity, we arrive at a final fermionic expression for the Hamiltonian

$$H = \frac{J}{2}\sum_{j=1}^{N-1} c_j^\dagger c_{j+1} + h.c + V\sum_{j=1}^{N-1} \rho_j \rho_{j+1} + \sum_{j=1}^{N} \mu_j \rho_j. \tag{14}$$

In the language of interacting fermions, the connection to the Anderson insulator becomes more transparent as we are able to see that switching off the interaction term, V, causes the system to describe a single particle hopping on a lattice.

4 Quantifying non-ergodic behaviour

To test whether or not the system is behaving ergodically or evading thermalisation, two key properties are considered. First; the growth and saturation of the entanglement entropy between a bi-partitioned system - and the entanglement entropy of the many-body eigenstates themselves. Secondly; the level spacing statistics of the many-body energy eigenvalues.

4.1 Entanglement entropy

As in the literature [15], we consider an equal bi-partition of the system with spins allocated to either sub-system A or B. Entanglement entropy gives a measure of how strongly correlated the degrees of freedom in sub-system A are with those in B. For a pure product state of the form,

$$|\Psi\rangle = \bigotimes_{j=1}^{N} |\phi_j\rangle \tag{15}$$

there are no correlations between each degree of freedom $|\phi_j\rangle$ as they exist independently of one another.

Conversely, consider the Bell state,

$$|\Psi\rangle = \frac{1}{\sqrt{2}}(|\uparrow\downarrow\rangle - |\downarrow\uparrow\rangle) \tag{16}$$

there is no pure state representation and so conclude that such states are entangled.

To mathematically verify this, we use the Von-Neumann entropy defined at a time t,

$$S_{VN}(t) = -Tr(\rho(t)log(\rho(t))) \tag{17}$$

where $\rho(t)$ is the density matrix for a given sub-system defined as

$$\rho(t) = |\Psi(t)\rangle \langle\Psi(t)| . \tag{18}$$

To consider the propagation of entanglement entropy across the system, we bipartition the system into two equal length chains, A and B, each containing $N/2$ spins. To do this, we trace out the degrees of freedom contributed from B,

$$\rho_A(t) = TR_B(\rho(t)) \tag{19}$$

Using the definition of the Von-Neumann entropy in (17); we calculate the entanglement of A with respect to B. Hence, determining the strength of the correlations between the two subsystems.

For a thermal system, entanglement will propagate ballisatically [11], $(S_{VN} \propto t)$ and will saturate at a value dependent on the length of the chain. Given that the ETH states that a physical observable is described by its thermal expectation value, we expect that the reduced density matrix of a subsystem, A, will also have a thermal expectation value

$$\rho_A(t) = \rho_A(T) = \frac{1}{Z}e^{-\frac{H}{K_B T}} \tag{20}$$

for a temperature T where Z is subsystem A's partition function and K_B is Boltzmann's constant. This relation allows us to infer that the entanglement entropy for a ther-

mal system is given by Gibbs' thermodynamic entropy, $S = -K_B \sum_i p_i log(p_i)$, in the thermodynamic limit. This definition of entropy is understood to be associated with the counting of states at a temperature T, and thus scales with the volume of the system. Employing this correspondence, we recognise that the entanglement entropy should also follow a volume scaling law when obeying the ETH. For 1-D systems, volume is simply length.

To evaluate entanglement entropy, we re-express the many-body wavefucntion in terms of basis elements from subsystems A and B.

$$|\Psi\rangle = \sum_{ij} \chi_{ij} |\varphi_i\rangle_A |\Phi_j\rangle_B \qquad (21)$$

As an example, consider a bipartitioned system with A containing two spins and B containing one,

$$\text{Basis}_A = \text{span}(|\uparrow\uparrow\rangle, |\uparrow\downarrow\rangle, |\downarrow\uparrow\rangle, |\downarrow\downarrow\rangle) \qquad (22)$$

$$\text{Basis}_B = \text{Span}(|\uparrow\rangle, |\downarrow\rangle)$$

which, in the computational basis, are expressed as the eigenvectors of the 2^N dimensional identity matrix.

Next, we write out the full form of the vector, in its computational basis, as a matrix whose columns are given by the degrees of freedom contributed from subsystem A and whose rows are described by the degrees of freedom contributed from subsystem B.

$$|\Psi\rangle = (a, b, c, d, e, f, g, h) = \qquad (23)$$

$$= \begin{matrix} & |\uparrow\uparrow\rangle & |\uparrow\downarrow\rangle & |\downarrow\uparrow\rangle & |\downarrow\downarrow\rangle \\ |\uparrow\rangle & \begin{pmatrix} a & c & e & g \\ |\downarrow\rangle & b & d & f & g \end{pmatrix} \end{matrix}$$

Note the composition of these vectors is of the form $|\uparrow\downarrow\uparrow\rangle = |\uparrow\downarrow\rangle \otimes |\uparrow\rangle$, which, for this vector in the computational basis, is unity in the 3rd entry and 0 everywhere else. I.e., the third component of the wavefunction, with the coefficient c.

To calculate the density operator, we perform a Schmidt decomposition on the wavefunction described by (21) by first considering the full density operator

$$\rho = |\Psi\rangle \langle \Psi| \qquad (24)$$

and observing that if $|\Psi\rangle$ is a pure state then it may be written as

$$|\Psi\rangle = |\varphi_A\rangle \otimes |\phi_B\rangle \qquad (25)$$

Otherwise, it may be more generally expressed as (21) with the coefficient χ_{ij} given as the overlap of the full many-body state with respect to the sub-system basis vectors; $\chi_{ij} = \langle\varphi_i| \otimes \langle\Phi_j|\Psi\rangle$.

Now perform a unitary transformation on the basis elements:

$$|\widetilde{\varphi_i}\rangle = \mathcal{U} |\varphi_i\rangle \text{ and } \left|\widetilde{\Phi_j}\right\rangle = \mathcal{V} |\Phi_j\rangle \qquad (26)$$

These rotations allow us to redefine the overlap coefficient

$$\widetilde{\chi_{ij}} = \langle\tilde{\varphi_i}| \otimes \langle\widetilde{\Phi_j}| |\Psi\rangle = \qquad (27)$$

$$= \langle\varphi_i| \mathcal{U}^\dagger \otimes \langle\Phi_j| \mathcal{V}^\dagger |\Psi\rangle$$

To evaluate this expression, insert a resolution of the identity for each basis, $\sum_i |\phi_i\rangle \langle\phi_i| = \mathbb{I}$. Acknowledging that they are acting on separate Hilbert spaces; we may shuffle the basis vectors around the expression as such

$$\widetilde{\chi_{ij}} = \sum_{pq} \langle\phi_i|\mathcal{U}^\dagger |\varphi_p\rangle \langle\Phi_j| \mathcal{V}^\dagger |\Phi_q\rangle \langle\varphi_p| \otimes \langle\Phi_q|\Psi\rangle \qquad (28)$$

$$\implies \widetilde{\chi_{ij}} = [u\chi v]_{ij}$$

The Schmidt decomposition [13] of $|\Psi\rangle$ is given by this pair of unitary transformations, $\mathcal{U}, \mathcal{V}$, acting on a complex valued matrix, χ_{ij}. It is always possible [14] to find transformations which make the resultant $\widetilde{\chi_{ij}} = [u\chi v]_{ij}$ diagonal. These diagonal values, S_i, are strictly real and positive semi-definite [14]. An extension to this, is that it is always possible to deconstruct the state vector as

$$|\Psi\rangle = \sum_i \sqrt{\lambda_i} |\varphi_i^s\rangle \otimes |\Phi_i^s\rangle \qquad (29)$$

where $\lambda_i = S_i^2$ are the Schmidt coefficients and $|\varphi_i^s\rangle, |\Phi_i^s\rangle$ are representations of the subsystems' basis elements in the Schmidt basis.

Considering this realisation of the state vector and our definition of the reduced density matrix (RDM) (19), we are able to extract its eigenvalues,

$$\rho_A = Tr_B (|\Psi\rangle \langle \Psi|) = \qquad (30)$$

$$= Tr_B \left(\sum_{ij} \sqrt{\lambda_i}\sqrt{\lambda_j} |\varphi_i^s\rangle \langle\varphi_j^s| \otimes |\Phi_i^s\rangle \langle\Phi_j^s| \right) =$$

$$= \sum_i \lambda_i |\varphi_i^s\rangle \langle\varphi_i^s|$$

which are the Schmidt coefficients.

Relating this back to the earlier example, (23), in which the coefficients χ_{ij} are realised in the matrix and vector. Performing the Schmidt decomposition has the effect of diagonalising the matrix regardless of dimension. Evidence of entanglement can be found by considering the trace of the squared RDM, if $Tr\left(\rho^2\right) < 1$, the state is entangled. Use of the Schmidt decomposition permits extraction of coefficients with which to evaluate the Von-Neumann entropy defined in (17) as

$$S_{VN}^A = -\sum_i \lambda_i log(\lambda_i). \qquad (31)$$

4.2 Level spacing statistics

Much of the existing literature relating to MBL properties discusses how the level spacing statistics of the energy eigenvalues may serve as a barometer for localisation [7]. Oganesyan and Huse [18] analysed the distribution of adjacent eigenvalues by unfolding the spectrum

$$r_n = \frac{E_{n-1} - E_n}{E_n - E_{n+1}} \tag{32}$$

with r_n as our random variable and E_n our energy spectrum for the Hamiltonian of interest.

The distribution

$$P(r) = \frac{1}{R} \sum_n^R \langle \delta(r - r_n) \rangle \tag{33}$$

for a system able to thermalise in accordance with the ETH, is predicted to follow a generalised Gaussian ensemble [19] given by

$$P_{WD}(r) = \frac{1}{Z} \frac{(r + r^2)^\beta}{(1 + r + r^2)^{1 + \frac{3\beta}{2}}} \tag{34}$$

where $Z = \frac{8}{27}$ and $\beta = 1$ correspond to the Gaussian Orthogonal Ensemble (GOE) and $Z = \frac{4}{81} \frac{\pi}{\sqrt{3}}$ and $\beta = 2$ correspond to the Gaussian Unitary Ensemble (GUE). Such ensembles exhibit level repulsion as $P_{WD}(r \to 0) \approx r^\beta \to 0$. The tail of this distribution decays as $P_{WD}(r \to \infty) \approx \frac{1}{r^{2+\beta}}$. We interpret this repulsion as adjacent many-body eigenstates repulsing due to a "knowledge" of one another; suggesting that these states are highly similar and therefore correlated. This is consistent with the notion of a thermal phase in that adjacent eigenstates are highly similar.

Alternatively, for a system escaping the thermal regime, adjacent eigenstates are uncorrelated due to their localised nature and so do not exhibit appreciable energy eigenstate repulsion. It was demonstrated [18] that such systems' level spacing statistics are described by a Poisson distribution

$$P_{Poisson}(r) = \frac{1}{(1+r)^2} \tag{35}$$

which tends to $P_{Poisson}(r \to 0) \to 1$ and $P_{Poisson}(r \to \infty) \approx \frac{1}{r^2}$.

However, it must be noted that the Hamiltonian (5) conserves total spin in the z orientation as $[H, S^z_{Tot}] = 0$ [2] which means that there is a conserved current if one considers the whole Hilbert space. This would make the model appear integrable, even in the absence of strong disorder and so the energy eigenvalue level spacing statistics would erroneously appear Poissonian. To circumvent this, one can either restrict the Hilbert space to only consider one value of $S^z_{Tot} = \sum_i S^z_i$, which one would normally take to be 0 [2][4]. Alternatively, one may introduce another weak, local field acting transverse to the z orientation to remove this conserved quantity. By making this perturbation weak and uniform, the dynamics of the system are unaffected, as we shall see when considering numerics of MBL systems, and yet we should still be able to observe Wigner-Dyson level repulsion.

In the literature, the middle of the spectrum [15] is often more closely studied as this region of the energy spectrum corresponds to an energy density far from the ground state - therefore at a finite effective temperature. Given that we are in a highly non-thermal phase, we cannot use thermodynamic properties such as $1/T = \partial_E S$ to extract information about the temperature. Hence, for localised systems, the effective temperature of the system is given by the local energy density of the many-body eigenstates.

5 Numerical procedure

In order to gain numerical insight into these highly entangled and excited states, we perform a unitary time evolution on an arbitrary initial state

$$|\Psi(0)\rangle = \bigotimes_i^N (cos(\theta_i) |\uparrow\rangle + sin(\theta_i) |\downarrow\rangle) \tag{36}$$

where each θ_i is drawn from a uniform distribution between $(-\pi, \pi)$. This corresponds to a collection of random vectors on their own Bloch spheres..

Due to the conserved quantity, S^z_{Tot}, as discussed in [15] and [4], we must ensure that we are not exploring eigenstates with different S^z_{Tot}. We achieve this by introducing a small transverse field, $\sum_j^N \chi \sigma^x_j$ where $\chi = 0.1$ to break the symmetry. To demonstrate that the only effect of this is to reveal the Wigner-Dyson level spacing statistics, we have run all of our simulations both in the presence and absence of the field.

5.1 Unitary time evolution

The unitary time evolution operator we use to perform the quench is

$$\mathcal{U}(t) = e^{-iHt} \tag{37}$$

which may be decomposed into

$$\mathcal{U}(t) = \sum_j^{2^N} e^{-itE_j} |E_j\rangle \langle E_j| \tag{38}$$

via the spectral theorem. We consider time steps relative to the strength of the coupling, J with each step being either $\Delta t = \frac{J}{100}$ or $\Delta t = J$ depending on what we are considering. The former is used when determining the propagation of entanglement entropy throughout the system as dephasing was found to occur on relatively short time scales. Alternatively, the latter time scale is used to map out the long time dynamics of a given spin or to evaluate the time evolution of the irreducible correlator [2].

$$\langle \sigma^x_1 \sigma^x_N \rangle_c = \langle \sigma^x_1 \sigma^x_N \rangle - \langle \sigma^x_1 \rangle \langle \sigma_N \rangle \tag{39}$$

To see evidence of long-time coherence, we can consider the trajectory over a single realisation of a single spin site. A system experiencing strong localisation effects should see long time coherence of a local observable which is in direction contradiction with the ETH which demands relaxation to a thermal state in finite time.

We consider the transverse and longitudinal magnetisations of the σ_1 in addition to the irreducible correlator on the whole chain as defined in (39).
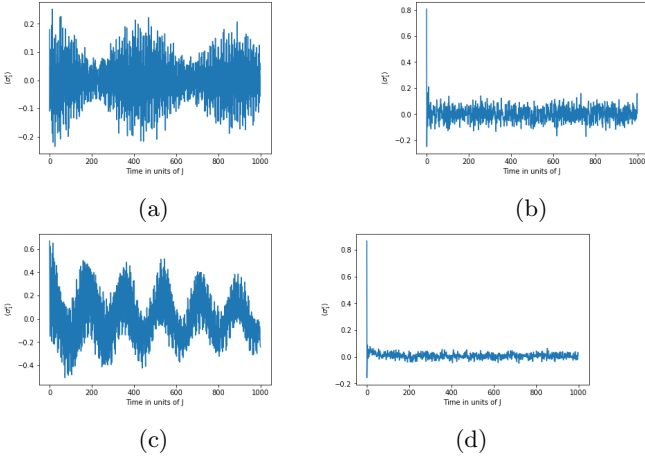
(a)

(b)

(c)

(d)

Figure 2: Unitary time evolution of $\langle \sigma_1^x \rangle$ with: **a**: $h = 10$ and $\chi = 0$. **b**: $h = 1$ and $\chi = 0$. **c**: $h = 10$ and $\chi = 0.1$. **d**: $h = 1$ and $\chi = 0.1$.

In figures (2.a) and (2.c), we see that the observables oscillate at many different frequencies with decaying envelope around a zero average. Moreover, this signal appears to have longevity relative to the size of J. These two, single realisation trajectories demonstrate behaviour consistent with resistance to thermal equilibration as the signal evades its thermal expectation value of zero for long times. In violation of the ETH. Conversely, inspection of figures (2.b) and (2.d) reveals rapid de-coherence towards the thermal expectation value for the local observable, consistent with the ETH.
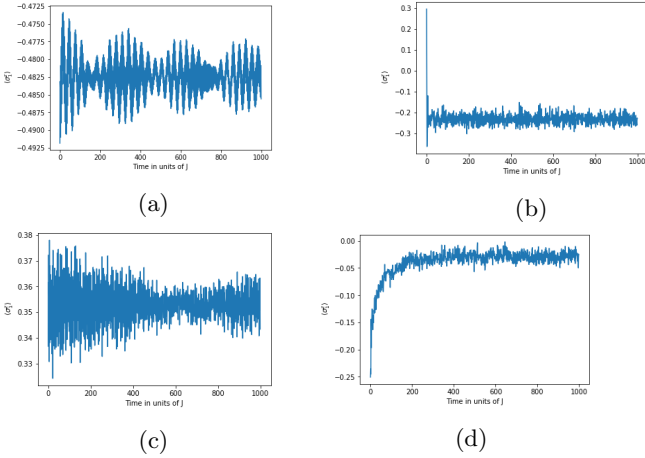

(a)

(b)

(c)

(d)

Figure 3: Unitary time evolution of $\langle \sigma_1^z \rangle$ with parameters set as: **a**: $h = 10$ and $\chi = 0$. **b**: $h = 1$ and $\chi = 0$. **c**: $h = 10$ and $\chi = 0.1$. **d**: $h = 1$ and $\chi = 0.1$.

We observe similar single trajectory dynamics for the local observable $\langle \sigma_1^z \rangle$ as we did for $\langle \sigma_1^x \rangle$, in that systems with overwhelming disorder display long-time coherence of a signal oscillating at many frequencies with a decaying envelope. Note that these trajectories are not averaged over many realisations, so that we may see how a single spin evolves during a single dynamical evolution. Consequently, each evolution may appear different, but the same fundamental properties are still visible. As before, we find that for a sufficiently weak random field, the system behaves ergodically and the local observables evolve towards their thermodynamic equi-

librium and do not oscillate far from this thermal state. We interpret the coherence of $\langle \sigma_1^z \rangle$ as a consequence of a non-trivial overlap with the conserved LIOM τ_1^z.
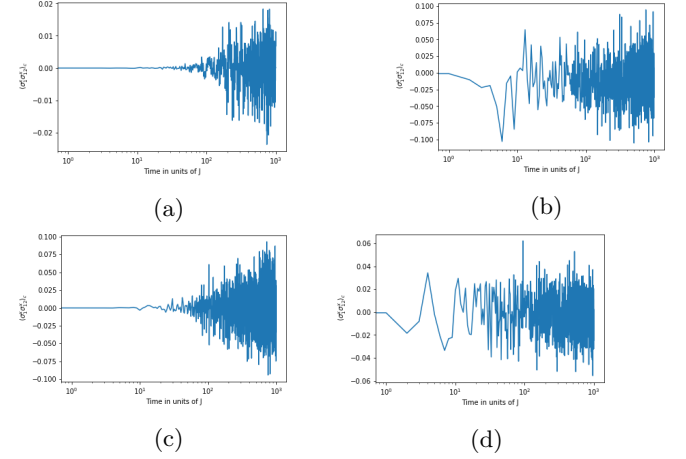

(a)

(b)

(c)

(d)

Figure 4: Unitary time evolution of the non-local observable $\langle \sigma_1^x \sigma_{12}^x \rangle_c$ with parameters set as: **a**: $h = 10$ and $\chi = 0$. **b**: $h = 1$ and $\chi = 0$. **c**: $h = 10$ and $\chi = 0.1$. **d**: $h = 1$ and $\chi = 0.1$.

The irreducible correlation function in the presence of strong disorder is strictly zero for short times due to the fact that our initial states are unambiguously product states. It then begins to oscillate away from zero on a time scale far shorter than the relaxation time of the local observables $\langle \sigma_1^x \rangle$ and $\langle \sigma_1^z \rangle$. This deviation may be caused by the exponentially decaying tails when relating the physical spins σ_i^z and the quasi-local, effective spins τ_i^z. Conversely, the lack of disorder allows correlations to propagate more freely across the chain and so correlations develop more strongly and over shorter time scales relative to a localised system.
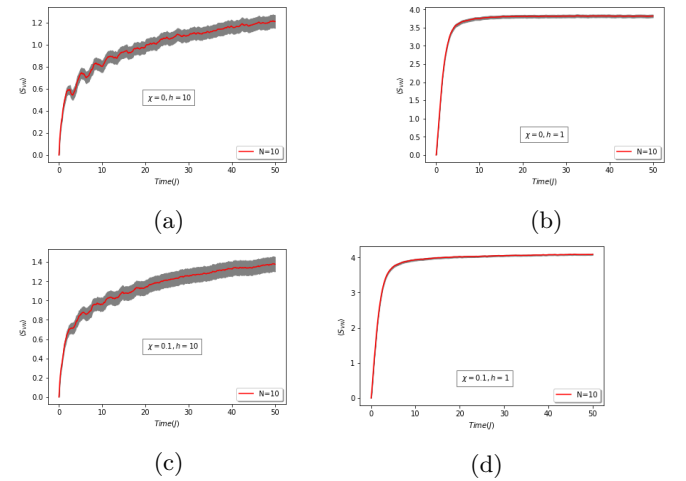

(a)

(b)

(c)

(d)

Figure 5: Unitary time evolution of the realisation averaged Von-Neumann entropy with: **a**: $h = 10$ and $\chi = 0$. **b**: $h = 1$ and $\chi = 0$. **c**: $h = 10$ and $\chi = 0.1$. **d**: $h = 1$ and $\chi = 0.1$.

Figure (5) supports the belief that thermal systems should support a ballistic spread of entanglement entropy and saturate in accordance with a volume scaling law. Alternatively, as seen in figs (5.a), (5.c), entropy saturates logarithmically in the MBL phase; and at a considerably smaller value than in the thermal phase. Given that entanglement

entropy is one of the key markers for ergodicity breaking in interacting systems, we my consider this to be reasonable evidence of such phenomena. We have only computed entropy growth for 10 interacting spins as the computational routine for performing Schmidt decomposition was numerically unstable for larger systems. Curves are averaged over 1000 realisations.

When calculating errors, we considered only the standard deviation error incurred over the realisations by using the maximum likelihood estimator (MLE) for the variance over realisations. From this, we then gave the error as the standard error for the procedure

$$\hat{\sigma}^2 = \frac{1}{N} \sum_{i=1}^{N} \left(S_{VN}^{(i)} - \overline{S_{VN}} \right)^2 \;\Rightarrow\; e = \pm \frac{\hat{\sigma}}{\sqrt{N}}. \qquad (40)$$

For the spread of entropy, we have plotted the standard error as the grey area surrounding the entropy curve.

5.2 Eigenstate entanglement entropy

As was discussed earlier, we expect that a thermal state should follow a volume law for the size of its entanglement entropy and a localised state should obey an area law [17][7][8]. In one dimension, we observe that the size of the boundary can only ever be constant as it will be the interface between the links of the subdivided chain; hence we expect the entanglement entropy for a chain of any length to exhibit the same entanglement entropy when localised.

To verify this, we generated a Hamiltonian of the form (5), with h ranging between 0 and 10 in increments of 0.25. We extracted the many body eigenstates and considered only those in the energy density range of $\epsilon \in \left(\frac{E_{Max}}{4}, \frac{3E_{Max}}{4} \right)$ where $\epsilon = \frac{E - E_{Min}}{E_{Max} - E_{Min}}$ and E_{Max}, E_{Min} are respectively the maximum and minimum energy eigenvalues. This is because we are principally concerned with the many-body eigenstates found in the middle of the spectrum as such states are expected to act fully thermally in accordance with the ETH and so evidence of ergodicity breaking shall be easier to detect in this region.

To compute the entanglement entropy of each eigenstate on the half chain, we made use of the protocol outlined in (4.1) and calculated the mean entanglement entropy for all of the eigenstates in the specified energy density interval. This mean was computed for each value of h over a total of 100 realisations. For each realisation, the randomised disorder in the Hamiltonian was redrawn.

In order to demonstrate the intensive nature of eigenstate entanglement entropy in the localised regime, we considered several spin chain lengths of N=4, 6, 8, and 10.
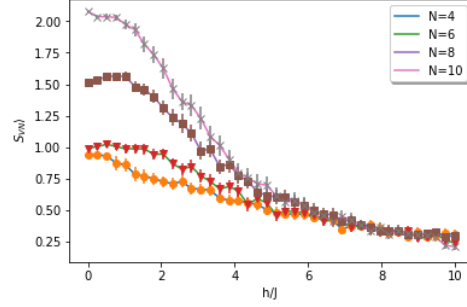

Figure 6: Average eigenstate entanglement entropy on the half chain against strength of disorder in the system. J=1, U=0.5.

Figure (6) illustrates the transition from a system whose entropy scales extensively to that of one scaling intensively with the transition occurring at approximately h=4 although there is a sharp decline in eigenstate entanglement entropy at approximately h=3.5. This is consistent with the literature [2] in that a critical disorder strength, h_c was determined to be ≈ 3.5.
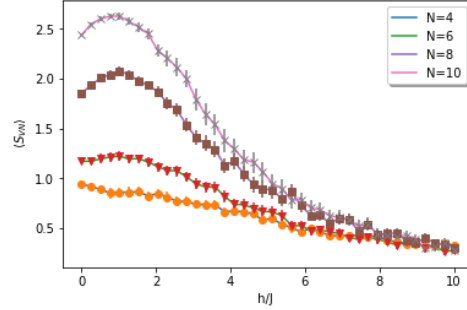

Figure 7: Average eigenstate entanglement entropy on the half chain against strength of disorder in the system. J=1, U=0.5, and χ=0.1.

Here, we have introduced a small transverse perturbation to the Hamiltonian as discussed in (4.2) to break the symmetry of total magnetisation. We have plotted this to demonstrate that the eigenstate dynamics of both phases are unaffected by the introduction of this perturbing field. We observe the transition from the thermal regime to the MBL regime for the same value of h, as evidenced by the transition from an extensive volume scaling law to an intensive area scaling law. As before, we calculate the errors on these entanglement entropy plots by using the standard error over all realisations.

## 5.3 Level spacing statistics

As discussed in section (5.2), one signature of a thermal phase is the adherence of its energy eigenvalue level spacing. A fully thermal phase experiences Wigner-Dyson eigenvalue repulsion whereas a localised phase has no such repulsion and enjoys a poissonian distribution for its eigenvalue spacing. We can plot the histograms for the level spacing as described in (32) and overlay curves to demonstrate suitability of fit.
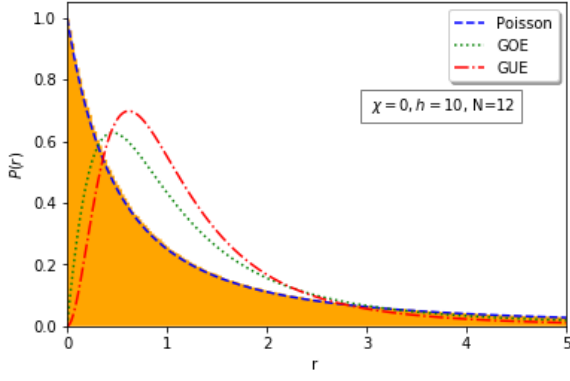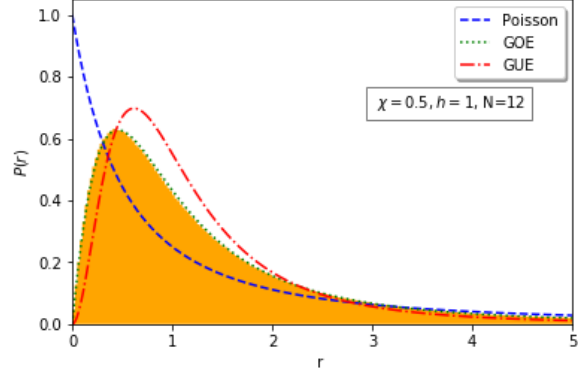
(a)
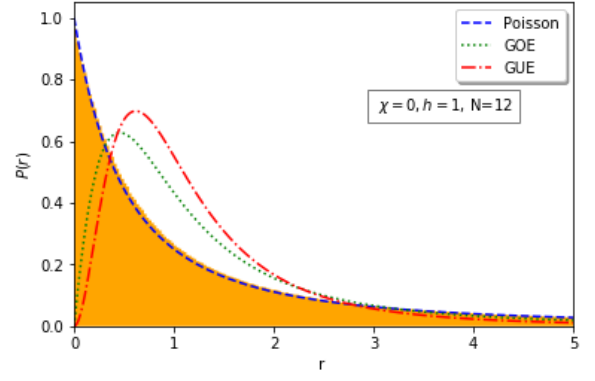
(b)
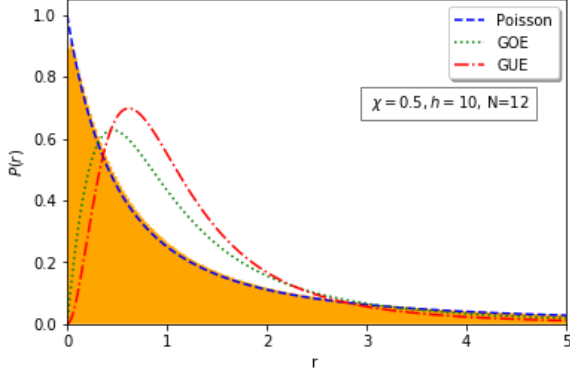
(c)

(d)

Figure 8: Empirical level spacing distributions extracted from simulated data compared against theoretical Wigner-Dyson distributions and the Poisson distribution. Orange block is the average of 2000 histograms within the specified energy density.
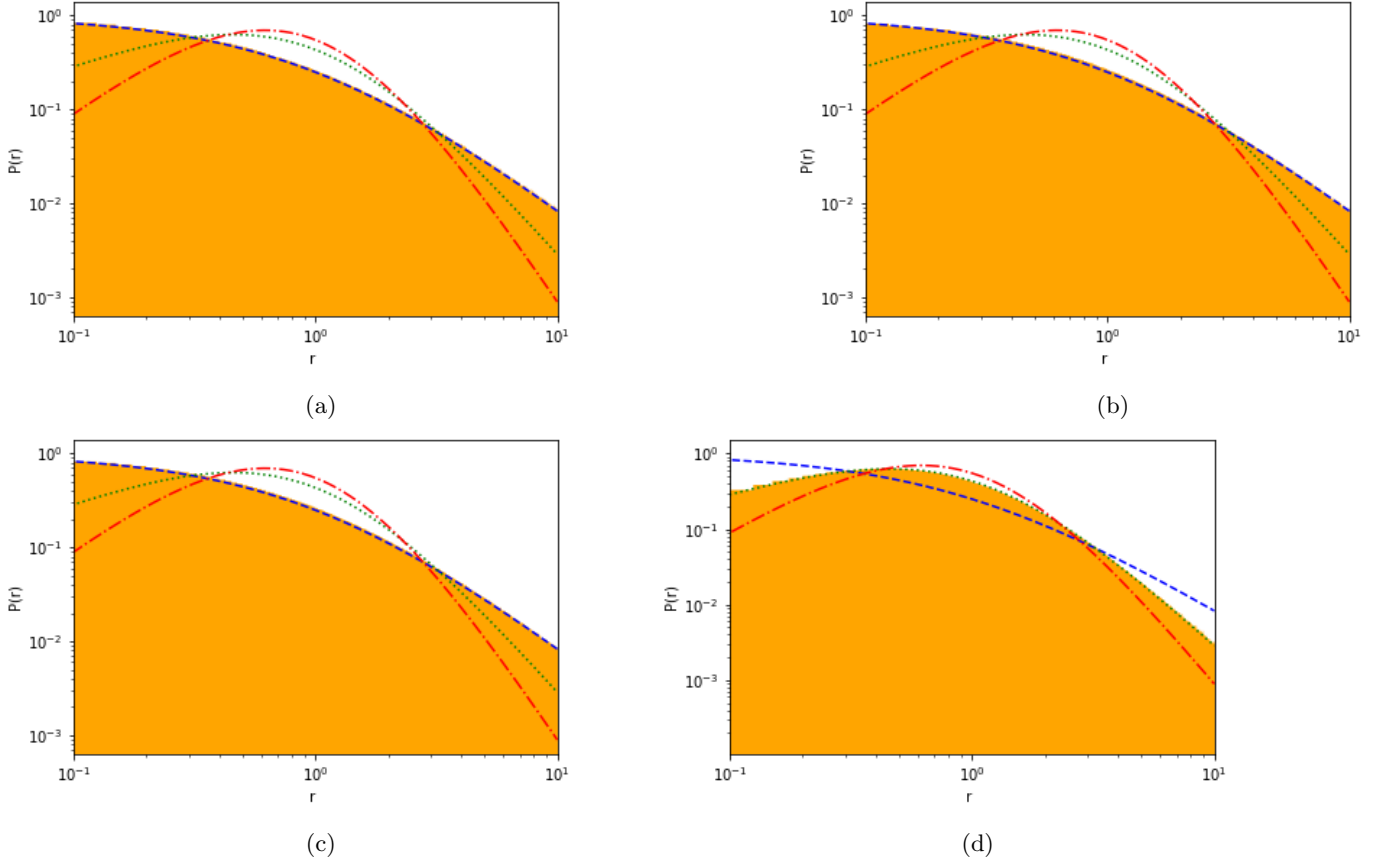
9

(a)

(b)

(c)

(d)

Figure 9: Log-Log plots of the empirical level spacing distributions extracted from simulated data compared against theoretical Wigner-Dyson distributions and the Poisson distribution. Orange block is the average of 2000 histograms within the specified energy density. Subfigures **a**, **b**, **c**, and **d** correspond to the same subfigure labels in figure 8.

As before, we consider the introduction of a weak, uniform transverse field to break the additional conservation law. Whereas before, this field had minimal effect on the dynamics or entanglement properties of the system, we find that in the absence of such a perturbation, the system may erroneously appear to be integrable dispute being firmly in the thermal regime. This corroborates the assertions of [15] and [4], in that the residual global conserved current of the Hamiltonian will result in misidentifying the phase.

To quantify the level of agreement between the empirical and theoretical distributions, we have calculated the normalised root mean squared error in linear space in order to calculate the percentage uncertainty. Moreover, we have calculated the χ^2 statistic for each distribution and the curve which it appears to fit most comfortably. For Pearson's χ^2 test, we have approximated our degrees of freedom to be the number of histogram bins, 1000, and are using a 95% confidence interval to accept or reject the null hypothesis that this is indeed the correct distribution. Data tables for the χ^2 distribution with DF=1000 state that we require a value of $\chi^2 < 1074.679$ [27] to accept the fit.

	Subfigures			
	8.a	8.b	8.c	8.d
χ^2	33.1	33.3	33.2	55.5
$\sqrt{\langle x_{Emp} - x_{Theo}\rangle}\%$	18.2	18.5	18.3	23.1

Figure 10: Summary of χ^2 statistics and percentage RMS error for each linear space histogram.

It is suspected that a large RMS error may be a consequence of truncating the distribution at $r = 5$ and not considering the whole length of the distribution as $r \to \infty$. It is not well understood how quickly the empirical distribution converges exactly onto the theoretical distribution. However; inspection of the agreement of fit in conjunction with the remarkable χ^2 agreement is sufficient substantiating evidence that thermal systems follow a Wigner-Dyson surmise and MBL systems - a Poisson distribution. As we see, there is remarkable agreement between the plotted histograms when $h = 10$ and the Gaussian Orthogonal Ensemble (GOE) curve, this has an expectation value of $\langle r_n \rangle_{GOE} \approx 0.5307$. Alternatively, when $h = 1$, we see that the distribution fits a Poisson curve, which has expectation value $\langle r_n \rangle_P \approx 2log(2) - 1 \approx 0.386$. We plot the arithmetic

mean of all of the calculated level spacings over all of the realisations at a given h. Moreover, we also calculate the standard error to predict possible deviation from the mean.

Moreover, in plotting the mean level spacing $\langle r_n(h) \rangle$, we may begin to gain insight into the nature of the transition.
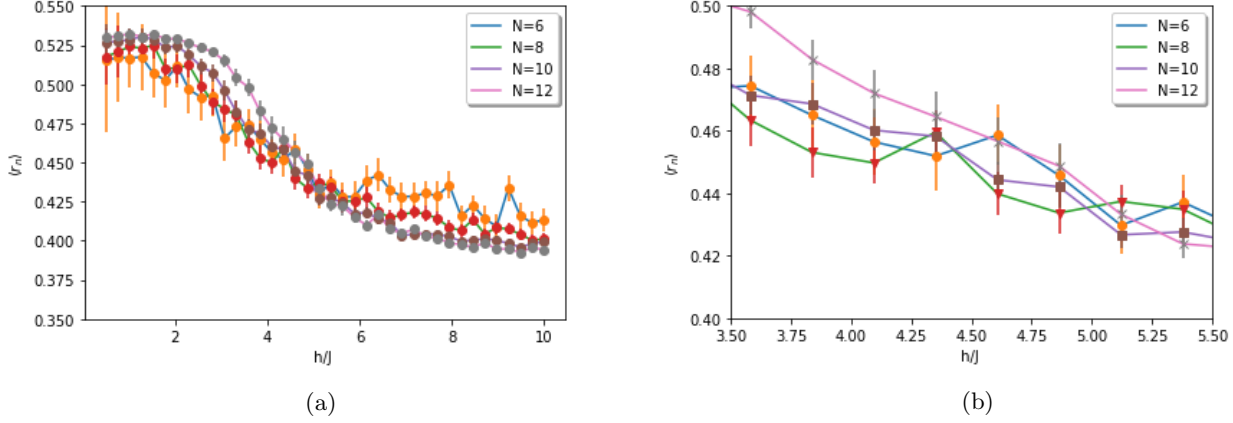

(a)

(b)

Figure 11: Mean value, $\langle r_n \rangle$, of the level spacing random variable as the random magnetic field is varied. Both subfigures are plotted with $\chi = 0.1$. **b**: Zooming in on the section in which the system begins to transition from the ergodic thermal phase to the non-ergodic many-body localised phase.
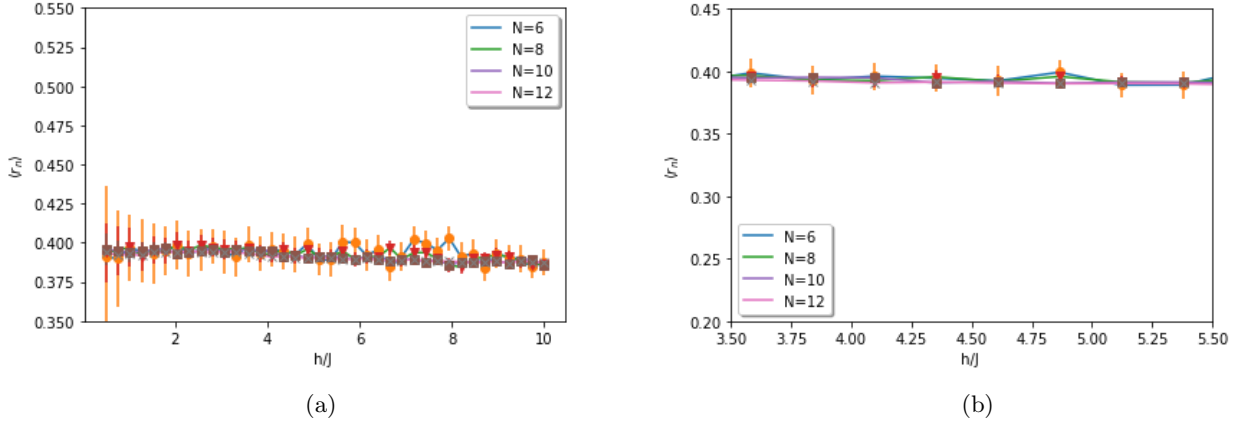

(a)

(b)

Figure 12: Mean value, $\langle r_n \rangle$, of the level spacing random variable as the random magnetic field is varied. Both subfigures are plotted with $\chi = 0$. **b**: Close up of the same region in fig(11.b) and no evidence of a transition.

Given the predictions made about the expectation values of the respective distributions, we observe a transition from a phase obeying GOE statistics to one following Poisson statistics, with this transition beginning around $h \approx 3.5$. Data has been averaged over 100 realisations for each h. Error bars on the y axis are given by standard sampling error. Note that we find curves are smoother and less sporadic for larger chains, this is due to the exponential scaling of the system. Examination of fig(11.b) demonstrates that even at disorder $h \approx 5.5$, we are not fully localised if we are using $\langle r_n \rangle$ as a barometer for the phase.

Conversely, we have no evidence of a phase transition in the absence of an additional $\chi \neq 0$ term as is evidenced in

fig(12). This is consistent with figures (8.b) and (9.b) and the predictions of [4][15].

6 Conclusions

Throughout this work, we have explored the features of thermalising quantum systems as well as systems capable of evading thermalisation via localisation. MBL physics is exciting to both theorist and experimentalist due to its unique properties and realisability in a laboratory [25][24].

Analytically, we have demonstrated that the XXZ model can be non-locally mapped to a series of interacting fermions

via the Jordan-Wigner transform which may provide an alternative platform from which to consider localisation. Moreover, we have borrowed techniques from quantum information theory to evaluate the entanglement entropy across our spin chains and demonstrated their applicability in such systems.

By considering the unitary time evolution of such systems, we have been able to gain insight into long-time coherence of local observables and the spread of correlations across the full chain. We have also considered the spread and growth rates of entanglement entropy within the system by using the methods derived from quantum information theory. Furthermore, we have examined the entanglement entropy of the many-body eigenstates to observe local and thermal behaviour; principally that a localised system is predicted to exhibit area law scaling of entropy whereas a thermal system is predicted to scale with the system's volume. We considered the average entropy for the many-body eigenstates in the middle of the energy spectrum and considered how this average varied with increased randomness. In doing so, we corroborated results from the literature by observing that eigenstate entanglement entropy for any chain length will converge to the same constant; consistent with an area law in 1D.

Finally, we plotted the probability distribution for the level spacing statistics of the energy eigenvalues deep in both the thermal and localised phases. The distributions showed astonishing agreement with the distributions predicted in the literature with means found in the appropriate places.

References

[1] P. W. Anderson, Phys. Rev. 109:1492-505 (1958)

[2] D. A. Abanin, and Z. Papic, Annalen der Physik 529 (7) (2017) 1700169, 1700169. doi:10.1002/andp.201700169.

[3] R. Nandkishore, and D. A. Huse, Annual Review of Condensed Matter Physics. (2015) 6: 15-38

[4] F. Alet, N. Laflorencie, Comptes Rendus Physique Volume 19, Issue 6, September–October 2018, Pages 498-525

[5] M. Serbyn, Z. Papic, D. A. Abanin, Phys. Rev. B *90*, 174302 (2014)

[6] J. Smith, et al, Nature Physics volume 12, pages 907–911 (2016)

[7] D. J. Luitz, and Y. B. Lev, Annalen der Physik **529** (7) (2017) 1600350, 1600350. doi:10.1002/andp.201600350.

[8] M. Serbyn, Z. Papic, and D. A. Abanin, Phys. Rev. Lett. **110**, 260601 (2013)

[9] C. Monthus, Journal of Statistical Mechanics, 2016, 2016, pp.033101

[10] A. Atland, and B. Simons: *Condensed Matter Field Theory, Second Edition*, Cambridge University Press (2010)

[11] G. Vitagliano, A. Riera, and J. I. Latorre, New Journal of Physics **12** 113049 (2010)

[12] A.V. Mikhailov, *Symmetries of Differential Equations and the Problem of Integrability.* Lect. Notes Phys. **767**, 19–88 (2009)

[13] E. Schmidt: Math. Ann. **63**, 433 (1907)

[14] P. A. Horn and C. R. Johnson: *Matrix Analysis* (Cambridge University Press, New York 1985)

[15] Z. Yang, A. Hamma, S. M. Giampaolo, E. R. Mucciolo, and C. Chamon, Phys. Rev. B **96**, 020408(R) (2017)

[16] J. Z. Imbrie, J. Stat. Phys. (2016) 163:998–1048

[17] J. Eisert, M. Cramer, and M. B. Plenio, Reviews of modern physics, **82**, (2010)

[18] V. Oganesyan and D. A. Huse, Phys. Rev. B **75** 155111 (2007)

[19] Y. Y. Atas et al., Phys. Rev. Lett. **110** 084101 (2013)

[20] J. Z. Imbrie, V. Ros, and A. Scardicchio, Annalen der Physik *529*, (7) 1600278 (2017) / DOI 10.1002/andp.201600278

[21] K. X. Wei, C. Ramanathan, and P Cappellaro, Phys. Rev. Lett. **120**, 070501 (2018)

[22] L. Rademaker, and M. Ortuno, Phys. Rev. Lett. **116**, 010404 (2016)

[23] T. E. O'Brien, D. A. Abanin, G. Vidal, and Z. Papic, Phys. Rev. B **94**, 144208 (2016)

[24] M. Schreiber, et al., Science 21 Aug 2015: Vol. 349, Issue 6250, pp. 842-845

[25] G. Kucsko, et al., Phys. Rev. Lett. **121**, 023601 (2018)

[26] T. Grover, and M. P. A. Fisher, J. Stat. Mech. P10010 (2014)

[27] https://www.medcalc.org/manual/chi-square-table.php Accessed 13:46 06/04/2019